

Human Physical Interaction based on UAV Cooperative Payload Transportation System using Adaptive Backstepping and FNTSMC

Hussein Naser, Hashim A. Hashim, and Mojtaba Ahmadi

Abstract—This paper presents a nonlinear control strategy for an aerial cooperative payload transportation system consisting of two quadrotor UAVs rigidly connected to a payload. The system includes human physical interaction facilitated by an admittance control. The proposed control framework integrates an adaptive Backstepping controller for the position subsystem and a Fast Nonsingular Terminal Sliding Mode Control (FNTSMC) for the attitude subsystem to ensure asymptotic stabilization. The admittance controller interprets the interaction forces from the human operator, generating reference trajectories for the position controller to ensure accurate tracking of the operator’s guidance. The system aims to assist humans in payload transportation, providing both stability and responsiveness. The robustness and effectiveness of the proposed control scheme in maintaining system stability and performance under various conditions are presented.

I. INTRODUCTION

AERIAL cooperative payload transportation using multiple UAVs is a growing field with significant potential in various applications [1], such as disaster relief scenarios, construction and industrial operations, and agriculture [1]–[4]. Robust adaptive estimators and control techniques for UAVs addressing uncertainties, ensuring synchronization, and rejecting disturbances are in high demand [1], [5]. Researchers have investigated different methods for grasping and transporting payloads cooperatively, such as suspended payloads [6] and aerial grasping manipulators [7], [8]. For suspended payloads, researchers in [6], developed a two quadrotors system to transport a beam-shaped payload. The quadrotors and the payload were considered as a single system and modeled using virtual structure approach. On the other hand, in [7] a leader-follower setting was implemented for cooperative transportation of payloads by a team of aerial manipulators. In the leader-follower paradigm, the leader is preprogrammed to navigate through a predefined path, while all other followers attempt to maintain their relative pose with respect to the leader. In [8], a cooperative transportation system using multiple aerial manipulators was developed. An adaptive controller and an online estimation method were proposed to estimate the mass of an unknown payload and control the aerial manipulation system based on estimated parameters.

The ability to control multiple UAVs cooperatively to transport and manipulate payloads presents numerous challenges, particularly in ensuring precise control, stability, and safety [3], [9]–[12]. These challenges become even more complex when considering the physical interactions between the aerial vehicle and human operators. In [13], the authors proposed a haptic slung payload system that consists of five quadrotors connected to the payload by cables. The system can move the payload according to human user guidance in 3D space by applying forces to it. The system relies on inline tension sensors for force estimation using PID and admittance control to track the user’s haptic guidance. In [14], [15], a cooperative suspended-payload transportation system was developed. The system consists of a rigid triangle-shaped payload transported by multiple micro aerial vehicles (MAVs) using massless cables. The authors implemented an admittance controller for the human-robot interaction and a hierarchical nonlinear controller to control the multiple MAVs during the transportation and manipulation tasks.

To control cooperative payload transportation missions, researchers used PID controllers [16]. Linear control methods often fail due to the system nonlinear nature, the presence of external disturbances, and the need for real-time adaptability to change in environment [1], [3], [17], [18]. Also, incorporating human-physical interaction adds another layer of complexity to the control system. As a remedy, robust nonlinear control such as sliding mode control, backstepping, and adaptive control were investigated to stabilize the system, compensate for system uncertainties, reject external disturbances, and accommodate human physical interaction [11], [19], [20]. Although using cables in cooperative payload transportation is popular, low-cost, and simple to implement, it suffers from some limitations and drawbacks. Cable-suspended payloads oscillate during the transportation task, which affects the stability of the system and necessitates complex control algorithms to stabilize the system [11]. In addition, oscillation interferes with the human interaction input and makes it difficult to implement the admittance controller. Furthermore, cables and tethers can get entangled during the task and destabilize the system, causing potential system damage and decreasing the safety level of the human partner. On the other hand, using aerial manipulators has the advantage of grasping and manipulating the payload autonomously; however, it suffers from serious drawbacks such as high cost, energy consumption, and the added mass of the robotic arms.

This work was supported in part by the National Sciences and Engineering Research Council of Canada (NSERC), under the grants RGPIN-2022-04937.

H. Naser, H. A. Hashim, and M. Ahmadi are with the Department of Mechanical and Aerospace Engineering, Carleton University, Ottawa, Ontario, K1S-5B6, Canada (e-mail: hhashim@carleton.ca).

Contribution: Motivated by the above challenges, in this work a rigidly connected cooperative transportation payload system consisting of two quadrotors and a transported payload with human physical interaction is proposed. The rigid connection is advantageous compared to other configurations; It unifies the quadrotors dynamics and the payload as one rigid-system, eliminates the oscillation to provide precise measurements of the physical interactions, and increases the operator safety. For the system's control, the proposed approach combines the strengths of Backstepping control to ensure position subsystem stability, Fast Nonsingular Terminal Sliding Mode Control (FNTSMC) for robust performance and rapid attitude subsystem convergence, and the admittance controller to facilitate the intuitive human physical interaction. The integration of these control strategies enhance the overall system performance and stability while addressing the cooperative payload transportation key challenges.

The paper is organized as follows: Section II details the methodology, including preliminaries, problem formulation, and system dynamics. Section III presents the position, attitude, and admittance control designs and stability analysis. The simulation and numerical results are presented in Section IV. Finally, the conclusion is stated in Section V.

II. METHODOLOGY

This study addresses the problem of an aerial payload transportation system with human physical interaction using adaptive backstepping control for position regulation, FNTSMC for attitude stabilization, and an admittance controller for human interaction. The aerial system lifts the transported payload while the human operator can interact by applying force to the payload directly guiding the system in 3D space. The interaction forces are measured using two force-torque sensors attached at the point of contact between the quadrotors and the payload.

A. System Model

Assumption 1. *The following assumptions are considered:*

- *The system comprises of three distinct rigid bodies: two identical quadrotors with known physical characteristics and a rigidly attached beam-shaped payload.*
- *The system is symmetric along the X and Y axes.*

For the modeling purposes, we assign a world inertial reference frame $\mathcal{W}_I = \{O_I, X_I, Y_I, Z_I\}$, body-attached reference frames $L_p = \{o_p, x_p, y_p, z_p\}$, and $q_i = \{o_i, x_{q_i}, y_{q_i}, z_{q_i}\}$ attached to the CoM of the payload and the CoM each quadrotor, respectively, where $(i = 1, 2)$. Let $\Omega = [p, q, r]^T$ be the angular rates defined in the body-attached frame which is the same for all components of the system due to rigid connection in Assumptions 1, and $\Phi = [\phi, \theta, \psi]^T$ be the Euler angles (roll, pitch, and yaw) defined in \mathcal{W}_I describing the system's orientation. The rotation matrix from the body-attached frame to \mathcal{W}_I -frame is $R \in SO(3)$, where $RR^T = \mathbf{I}$ and $\det(R) = +1$ with \mathbf{I} being the identity matrix [18], [21].

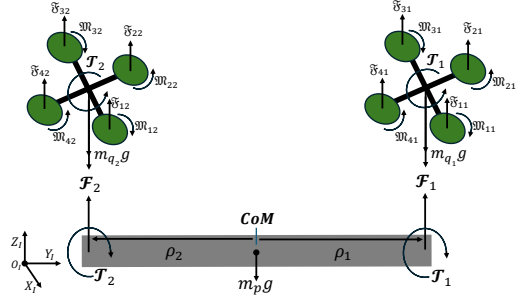


Fig. 1: Free body diagram of the entire system components.

1) *Quadrotor Dynamics:* Let $r_{q_i} = [x_{q_i}, y_{q_i}, z_{q_i}]^T$ be the position of the i^{th} quadrotor and $v_{q_i} = \dot{r}_{q_i}$ defined in \mathcal{W}_I . The underactuated UAV model dynamics are described according to the Newton-Euler method as follows [3], [11]:

$$\begin{aligned} m_{q_i} \dot{v}_{q_i} &= R\mathcal{F}_{q_i}e_z - m_{q_i}ge_z - \mathcal{F}_i \\ \mathcal{I}_{q_i} \dot{\Omega} &= \tau_{q_i} - \Omega \times \mathcal{I}_{q_i}\Omega - \mathcal{T}_i \end{aligned} \quad (1)$$

where $m_{q_i} \in \mathbb{R}$ and $\mathcal{I}_{q_i} \in \mathbb{R}^{3 \times 3}$ are the mass and moment of inertia, and $\mathcal{F}_i \in \mathbb{R}^3$ and $\mathcal{T}_i \in \mathbb{R}^3$ are the force and torque exerted by the i^{th} quadrotor on the attached payload, respectively, $g \in \mathbb{R}$ denotes the gravity, $e_z = [0, 0, 1]^T$ is a unit vector along z axis, and $\mathcal{F}_{q_i} \in \mathbb{R}$ and $\tau_{q_i} \in \mathbb{R}^3$ represents the thrust and the (rolling, pitching, and yawing) moments measured in the body-attached frame, such that:

$$\begin{bmatrix} \mathcal{F}_{q_i} \\ \tau_{q_i} \end{bmatrix} = \begin{bmatrix} \mathfrak{F}_{i1} + \mathfrak{F}_{i2} + \mathfrak{F}_{i3} + \mathfrak{F}_{i4} \\ d(\mathfrak{F}_{i2} - \mathfrak{F}_{i4}) \\ d(\mathfrak{F}_{i3} - \mathfrak{F}_{i1}) \\ \mathfrak{M}_{i1} - \mathfrak{M}_{i2} + \mathfrak{M}_{i3} - \mathfrak{M}_{i4} \end{bmatrix} \quad (2)$$

where $\mathfrak{F}_{ij} = k_f \omega_{ij}^2$ and $\mathfrak{M}_{ij} = k_m \omega_{ij}^2$ are the thrust and moment of each rotor per quadrotor, and k_f, k_m are the thrust and moment constants, respectively, ω_{ij} is the rotor angular speed, and d is the quadrotor's arm length.

2) *Payload Dynamics:* Let $r_p = [x_p, y_p, z_p]^T$ be the payload's CoM position and $v_p = \dot{r}_p$ is defined in \mathcal{W}_I . Referring to Fig. 1, the payload dynamics are formulated as follows:

$$\begin{aligned} m_p \dot{v}_p &= (\mathcal{F}_1 + \mathcal{F}_2) - m_pge_z \\ \mathcal{I}_p \dot{\Omega} &= (\mathcal{T}_1 + \mathcal{T}_2) - \Omega \times \mathcal{I}_p\Omega + (\rho_1 \times \mathcal{F}_1) + (\rho_2 \times \mathcal{F}_2) \end{aligned} \quad (3)$$

where $\dot{v}_p \in \mathbb{R}^3$ is the translational acceleration, $m_p \in \mathbb{R}$ and $\mathcal{I}_p \in \mathbb{R}^{3 \times 3}$ are the mass and moment of inertia, respectively. The terms $\rho_1 \times \mathcal{F}_1$ and $\rho_2 \times \mathcal{F}_2$ represent the moments exerted by the i^{th} quadrotor at the points of attachment, and $\rho_i = r_{q_i} - r_p$ represents the vectors between the payload's CoM and the i^{th} quadrotor.

3) *Entire Aerial Assistive System Dynamics:* Let $r_s = [x, y, z]^T$ be the entire aerial system's CoM position and $v_s = \dot{r}_s = [v_{s_x}, v_{s_y}, v_{s_z}]^T$ is the velocity defined in \mathcal{W}_I . Based on Assumption 1 and Fig. 1, integrating the dynamics of the quadrotors in (1) with the payload dynamics in (3) and including the aerodynamic drag effects, the dynamics of the entire system becomes:

$$\begin{aligned} m_s \dot{v}_s &= R\mathcal{U}_{th}e_z - m_sge_z - F_d \in \mathbb{R}^3 \\ \mathcal{I}_s \dot{\Omega} &= \mathcal{U}_m - \Omega \times \mathcal{I}_s\Omega - M_d \in \mathbb{R}^3 \end{aligned} \quad (4)$$

the admittance controller according to the applied forces of the human guidance. Let the position tracking error be:

$$E_p = \begin{bmatrix} E_{px} \\ E_{py} \\ E_{pz} \end{bmatrix} = \begin{bmatrix} x_d - x \\ y_d - y \\ z_d - z \end{bmatrix} \in \mathbb{R}^3 \quad (13)$$

The time derivative of (13) is:

$$\dot{E}_p = \begin{bmatrix} \dot{E}_{px} \\ \dot{E}_{py} \\ \dot{E}_{pz} \end{bmatrix} = \begin{bmatrix} \dot{x}_d - \dot{x} \\ \dot{y}_d - \dot{y} \\ \dot{z}_d - \dot{z} \end{bmatrix} = \begin{bmatrix} \dot{x}_d - \nu_{s_x} \\ \dot{y}_d - \nu_{s_y} \\ \dot{z}_d - \nu_{s_z} \end{bmatrix} \quad (14)$$

Let \odot and \odot^2 be the elementwise multiplication and exponentiation operators, respectively. Based on (13) and (14), let the following vector of scalar functions, $V_p = \frac{1}{2}E_p^{\odot 2}$ be Lyapunov function candidates where $V_p = [V_{px}, V_{py}, V_{pz}]^T$. Taking the time derivative of V_p , such that:

$$\dot{V}_p = E_p \odot \dot{E}_p = E_p \odot \begin{bmatrix} \dot{x}_d - \nu_{s_x} \\ \dot{y}_d - \nu_{s_y} \\ \dot{z}_d - \nu_{s_z} \end{bmatrix} \quad (15)$$

Consider $X_{temp} = [\nu_{s_{xd}}, \nu_{s_{yd}}, \nu_{s_{zd}}]^T \in \mathbb{R}^3$ as a temporary desired control input used to ensure asymptotic stability of the position, such that:

$$X_{temp} = K_p E_p + \dot{X}_d \in \mathbb{R}^3 \quad (16)$$

where $X_d = [x_d, y_d, z_d]^T$ and $K_p \in \mathbb{R}^{3 \times 3} = \text{diag}(k_{p1}, k_{p2}, k_{p3}) > 0$. Substituting (16) into (15), one gets:

$$\begin{aligned} \dot{V}_p &= E_p \odot (\dot{X}_d - X_{temp}) = E_p \odot (\dot{X}_d - K_p E_p - \dot{X}_d) \\ &= -K_p E_p^{\odot 2} < 0, \quad \forall \text{ elements of } E_p \neq 0. \end{aligned} \quad (17)$$

Based on (17), the origin ($E_p = 0$) is globally asymptotically stable. As a second step, let E_v be the error between the X_{temp} and $X_{state} = [\nu_{s_x}, \nu_{s_y}, \nu_{s_z}]^T \in \mathbb{R}^3$ from (12) as follows:

$$E_v = \begin{bmatrix} E_{vx} \\ E_{vy} \\ E_{vz} \end{bmatrix} = (K_p E_p + \dot{X}_d) - X_{state} \quad (18)$$

Define $V_v = \frac{1}{2}E_p^{\odot 2} + \frac{1}{2}E_v^{\odot 2}$ as a vector of Lyapunov function candidates, where $V_v = [V_{vx}, V_{vy}, V_{vz}]^T$; take its time derivative, and substitute (18) into the result, such that:

$$\begin{aligned} \dot{V}_v &= E_p \odot \dot{E}_p + E_v \odot \dot{E}_v = E_p \odot (\dot{X}_d - X_{temp}) + \\ &E_v \odot [(K_p \dot{E}_p + \ddot{X}_d) - \dot{X}_{state}] \end{aligned} \quad (19)$$

Since we require the state variables X_{state} to track the temporary desired control input X_{temp} , therefore, equation (19) can be rearranged and simplified as follows:

$$\dot{V}_v = -K_p E_p^{\odot 2} + E_v \odot [-E_p + K_p \dot{E}_p + \ddot{X}_d - U_v - \mathcal{Q}_p] \quad (20)$$

where U_v is a virtual control of the position subsystem from (12), and it is given as follows:

$$U_v = \begin{bmatrix} u_{vx} \\ u_{vy} \\ u_{vz} \end{bmatrix} = \frac{1}{m_s} \begin{bmatrix} (s\theta c\psi + s\phi c\theta s\psi)\mathcal{U}_{th} \\ (s\theta s\psi - s\phi c\theta c\psi)\mathcal{U}_{th} \\ -m_s g + (c\phi c\theta)\mathcal{U}_{th} \end{bmatrix} \quad (21)$$

and $\mathcal{Q}_p = \frac{1}{m_s}[-k_{dl}\nu_{s_x}, -k_{dl}\nu_{s_y}, -k_{dl}\nu_{s_z}]^T$ represents the drag forces in (12). The virtual controller in (20) needs to

be designed to ensure the asymptotic stability of the system and the errors' convergence to the origin as follows:

$$U_v = \hat{K}_v E_v - E_p + K_p \dot{E}_p + \ddot{X}_d - \mathcal{Q}_p \quad (22)$$

where $\hat{K}_v \in \mathbb{R}^{3 \times 3} = \text{diag}(\hat{k}_{v1}, \hat{k}_{v2}, \hat{k}_{v3})$ represents the the adaptive controller's parameter to estimate the constant parameter $K_v \in \mathbb{R}^{3 \times 3} = \text{diag}(k_{v1}, k_{v2}, k_{v3}) > 0$ with the following adaptation law:

$$\dot{\hat{K}}_v = \mathcal{B} E_v^{\odot 2} \quad (23)$$

where $\mathcal{B} \in \mathbb{R}^{3 \times 3} = \text{diag}(\beta_1, \beta_2, \beta_3) > 0$. To ensure the stability of the position subsystem with the adaptation law in (23), let $V_{pv} \in \mathbb{R}^3$ be a Lyapunov function candidates as follows:

$$V_{pv} = \frac{1}{2}E_p^{\odot 2} + \frac{1}{2}E_v^{\odot 2} + \frac{1}{2}\mathcal{B}^{-1}\tilde{K}_v^2 \quad (24)$$

where ($\tilde{K}_v = K_v - \hat{K}_v$). Take the time derivative of (24), one gets:

$$\begin{aligned} \dot{V}_{pv} &= -K_p E_p^{\odot 2} - \hat{K}_v E_v^{\odot 2} + \mathcal{B}^{-1}\tilde{K}_v \dot{\hat{K}}_v \\ &= -K_p E_p^{\odot 2} - (K_v - \tilde{K}_v)E_v^{\odot 2} - \mathcal{B}^{-1}\tilde{K}_v \dot{\hat{K}}_v \\ &= -K_p E_p^{\odot 2} - K_v E_v^{\odot 2} + \tilde{K}_v (E_v^{\odot 2} - \mathcal{B}^{-1}\dot{\hat{K}}_v) \end{aligned} \quad (25)$$

Substituting (23) into (25), results in:

$$\dot{V}_{pv} = -K_p E_p^{\odot 2} - K_v E_v^{\odot 2} < 0, \quad \forall E_p \neq 0 \ \& \ E_v \neq 0 \quad (26)$$

by which the stability of the position is guaranteed according to the Lyapunov theory. Based on (22), the virtual controllers of the position subsystem are given as follows:

$$\begin{aligned} u_{vx} &= -E_{px} + \hat{k}_{v1}E_{vx} + k_{p1}\dot{E}_{px} + \ddot{x}_d - \mathcal{Q}_p(1) \\ u_{vy} &= -E_{py} + \hat{k}_{v2}E_{vy} + k_{p2}\dot{E}_{py} + \ddot{y}_d - \mathcal{Q}_p(2) \\ u_{vz} &= -E_{pz} + \hat{k}_{v3}E_{vz} + k_{p3}\dot{E}_{pz} + \ddot{z}_d - \mathcal{Q}_p(3) \end{aligned} \quad (27)$$

Based on (21), the total thrust of the entire system \mathcal{U}_{th} and the desired orientation angles (ϕ_d, θ_d) as outputs of the (outer loop) position controller are given as follows:

$$\begin{aligned} \mathcal{U}_{th} &= m_s \sqrt{u_{vx}^2 + u_{vy}^2 + (u_{vz} + g)^2} \\ \theta_d &= \arctan \left(\frac{u_{vx} \cos(\psi_d) + u_{vy} \sin(\psi_d)}{u_{vz} + g} \right) \\ \phi_d &= \arctan \left(\frac{\cos(\theta_d)(u_{vx} \sin(\psi_d) - u_{vy} \cos(\psi_d))}{u_{vz} + g} \right) \end{aligned} \quad (28)$$

B. Attitude Subsystem Controller

The attitude control of the system is managed by FNTSMC. This controller offers rapid convergence and robustness against uncertainties. The controller design process and the stability analysis according to Lyapunov theory are given follows:

1) *Sliding surface design*: Let $E_\Phi \in \mathbb{R}^3$ be the tracking error of the attitude subsystem which is given as:

$$E_\Phi = \begin{bmatrix} E_\phi \\ E_\theta \\ E_\psi \end{bmatrix} = \eta_{d\Phi} - \eta_\Phi = \begin{bmatrix} \phi_d - \phi \\ \theta_d - \theta \\ \psi_d - \psi \end{bmatrix} \quad (29)$$

Take the time derivative of (29), we get:

$$\dot{E}_\Phi = \dot{\eta}_{d\Phi} - \dot{\eta}_\Phi = \begin{bmatrix} \dot{\phi}_d - \dot{\phi} \\ \dot{\theta}_d - \dot{\theta} \\ \dot{\psi}_d - \dot{\psi} \end{bmatrix} \quad (30)$$

For the system in (11) and the tracking error in (29), the FNTSM surfaces of the attitude subsystem are chosen to be as follows:

$$S_\Phi = \dot{E}_\Phi + \zeta E_\Phi + \gamma \text{sgn}(E_\Phi)^\varepsilon \quad (31)$$

where $S_\Phi = [S_\phi, S_\theta, S_\psi]^\top \in \mathbb{R}^3$, $\zeta > 0$, $\gamma > 0$, $\varepsilon \geq 1$, $\text{sgn}(E_\Phi)^\varepsilon = |E_\Phi|^\varepsilon \text{sgn}(E_\Phi)$ and its derivative is given as [23] $\frac{d}{dt}(\text{sgn}(E_\Phi)^\varepsilon) = \varepsilon |E_\Phi|^{\varepsilon-1} \dot{E}_\Phi$, and $\text{sgn}(\cdot)$ is the sign function. The sliding surface time derivative in (31) is:

$$\begin{aligned} \dot{S}_\Phi &= \ddot{E}_\Phi + \zeta \dot{E}_\Phi + \gamma \varepsilon |E_\Phi|^{\varepsilon-1} \dot{E}_\Phi \\ &= \ddot{\eta}_{d\Phi} - \ddot{\eta}_\Phi + \zeta \dot{E}_\Phi + \gamma \varepsilon |E_\Phi|^{\varepsilon-1} \dot{E}_\Phi \end{aligned} \quad (32)$$

Substituting (11) into (32) results in:

$$\dot{S}_\Phi = \ddot{\eta}_{d\Phi} - \mathcal{Q}_\Phi(\eta) - b(\eta)\mathcal{U} + (\zeta + \gamma \varepsilon |E_\Phi|^{\varepsilon-1}) \dot{E}_\Phi \quad (33)$$

Considering $\hat{\mathcal{U}}$ as an equivalent controller (continuous control law) to achieve $\dot{S}_\Phi = 0$ consider the following expression:

$$\hat{\mathcal{U}} = \frac{1}{b(\eta)} \left[\ddot{\eta}_{d\Phi} - \mathcal{Q}_\Phi(\eta) + (\zeta + \gamma \varepsilon |E_\Phi|^{\varepsilon-1}) \dot{E}_\Phi \right] \quad (34)$$

To address the dynamic uncertainties and external disturbances, as well as to increase the speed convergence to the sliding surface, the control law can be formulated by incorporating a discontinuous term into $\hat{\mathcal{U}}$ in (34) as follows:

$$\mathcal{U} = \hat{\mathcal{U}} + \frac{1}{b(\eta)} [\kappa_1 S_\Phi + \kappa_2 \text{sgn}(S_\Phi)] \quad (35)$$

where $\kappa_1 > 0$ and $\kappa_2 > 0$. The attitude controller takes the desired roll and pitch angles (ϕ_d and θ_d) that are generated by the position controller in (28). The desired yaw angle ψ_d is set by the designer in view of the entire system configuration to generate the control law in (35) as follows:

$$\begin{aligned} \mathcal{U}_{m1} &= \mathcal{I}_{sx} [\ddot{\phi}_d - \mathcal{Q}_\Phi(1) + (\zeta_\phi + \gamma \varepsilon |E_\phi|^{\varepsilon-1}) \dot{E}_\phi + \\ &\quad \kappa_1 S_\phi + \kappa_2 \text{sgn}(S_\phi)] \\ \mathcal{U}_{m2} &= \mathcal{I}_{sy} [\ddot{\theta}_d - \mathcal{Q}_\Phi(2) + (\zeta_\theta + \gamma \varepsilon |E_\theta|^{\varepsilon-1}) \dot{E}_\theta + \\ &\quad \kappa_1 S_\theta + \kappa_2 \text{sgn}(S_\theta)] \\ \mathcal{U}_{m3} &= \mathcal{I}_{sz} [\ddot{\psi}_d - \mathcal{Q}_\Phi(3) + (\zeta_\psi + \gamma \varepsilon |E_\psi|^{\varepsilon-1}) \dot{E}_\psi + \\ &\quad \kappa_1 S_\psi + \kappa_2 \text{sgn}(S_\psi)] \end{aligned} \quad (36)$$

where

$$\mathcal{Q}_\Phi = \begin{bmatrix} \frac{1}{\mathcal{I}_{sx}} \left[-k_{dr} \dot{\phi} + (\mathcal{I}_{sy} - \mathcal{I}_{sz}) \dot{\theta} \dot{\psi} \right] \\ \frac{1}{\mathcal{I}_{sy}} \left[-k_{dr} \dot{\theta} + (\mathcal{I}_{sz} - \mathcal{I}_{sx}) \dot{\phi} \dot{\psi} \right] \\ \frac{1}{\mathcal{I}_{sz}} \left[-k_{dr} \dot{\psi} + (\mathcal{I}_{sx} - \mathcal{I}_{sy}) \dot{\phi} \dot{\theta} \right] \end{bmatrix}$$

C. Stability Analysis

Theorem 1. *Given the system dynamics outlined in (11) and the FNTSM surfaces specified in (31), the proposed control law in (35) guarantees asymptotic stability of the closed-loop system. Additionally, the system trajectories can reach to the equilibrium state on the FNTSM ($S_\Phi = 0$) within a finite time.*

Proof: To prove Theorem 1, let V_Φ be a Lyapunov function candidate as follows:

$$V_\Phi = \frac{1}{2} S_\Phi^{\odot 2}, \quad (V_\Phi \geq 0 \quad \forall \text{ elements of } S_\Phi) \quad (37)$$

The time derivative of (37) is:

$$\dot{V}_\Phi = S_\Phi \odot \dot{S}_\Phi \quad (38)$$

Substituting (33) into (38) results in the following:

$$\dot{V}_\Phi = \left[\ddot{\eta}_{d\Phi} - \mathcal{Q}(\eta) - b(\eta)\mathcal{U} + (\zeta + \gamma \varepsilon |E_\Phi|^{\varepsilon-1}) \dot{E}_\Phi \right] \odot S_\Phi \quad (39)$$

Substituting (35) into (39) results in the following:

$$\begin{aligned} \dot{V}_\Phi &= [-\kappa_1 S_\Phi - \kappa_2 \text{sgn}(S_\Phi)] \odot S_\Phi \\ &= -\kappa_1 S_\Phi^{\odot 2} - \kappa_2 |S_\Phi| \leq 0, \quad \forall S_\Phi \end{aligned} \quad (40)$$

which ensures asymptotic convergence. To prove convergence to the sliding surfaces ($S_\Phi = 0$) in a finite time, define t_r as the reaching time and let us rewrite (40) as follows:

$$\dot{V}_\Phi = \frac{dV_\Phi}{dt} = -\kappa_1 S_\Phi^{\odot 2} - \kappa_2 |S_\Phi| \quad (41)$$

Using (37), The expression in (41) can be rewritten as follows:

$$\frac{dV_\Phi}{dt} \leq -2\kappa_1 V_\Phi - \kappa_2 \sqrt{2V_\Phi}, \quad \text{s.t. } dt \leq \frac{-dV_\Phi}{2\kappa_1 V_\Phi + \alpha V_\Phi^{1/2}} \quad (42)$$

where $\alpha = \sqrt{2}\kappa_2$, then integrate both sides of (42) such that:

$$\int_0^{t_r} dt \leq \int_{V_\Phi(0)}^{V_\Phi(t_r)} \frac{-dV_\Phi}{2\kappa_1 V_\Phi + \alpha V_\Phi^{1/2}} \quad (43)$$

Integrating (43) shows that the reaching time (t_r) can be calculated as:

$$t_r \leq \frac{1}{\kappa_1} \ln \left| \frac{2\kappa_1 V_\Phi(0)^{1/2} + \alpha}{\alpha} \right| \quad (44)$$

Based on (44), the system trajectories will reach ($S_\Phi = 0$) and the errors will converge to the origin within a finite time.

D. Admittance Controller for Human Physical Interaction

The admittance controller facilitates physical interaction between the human operator and the aerial system. It measures the interaction forces and generates reference trajectories for accurate tracking. The admittance controller simulates a mass-damper-spring system by modifying virtual inertia, damping, and stiffness of the robotic system as given in the following mathematical relationship (45):

$$\mathcal{M}(\ddot{\mathcal{R}}_d - \ddot{\mathcal{R}}_r) + \mathcal{C}(\dot{\mathcal{R}}_d - \dot{\mathcal{R}}_r) + \mathcal{K}(\mathcal{R}_d - \mathcal{R}_r) = \mathcal{F}_h \quad (45)$$

where: $\mathcal{M} \in \mathbb{R}^{3 \times 3}$, $\mathcal{C} \in \mathbb{R}^{3 \times 3}$, $\mathcal{K} \in \mathbb{R}^{3 \times 3}$ are diagonal matrices of the virtual mass, damping, stiffness, respectively, $\mathcal{R}_d \in \mathbb{R}^3$ is the desired trajectory, $\mathcal{R}_r \in \mathbb{R}^3$ is the reference

TABLE I: System and Controller parameters.

Symbol	Definition	Value/ Unit
m_{q_i}, m_p, m_s	Masses (quad., load, total)	(1.4, 0.45, 3.25)/kg
d	Arm length of i^{th} quad.	0.225/m
l_p	Length of payload	2.2/m
g	Gravitational acceleration	9.81/m/s ²
\mathcal{I}_{sx}	Moment of inertia in x-axis	3.039/kg m ²
\mathcal{I}_{sy}	Moment of inertia in y-axis	0.051/kg m ²
\mathcal{I}_{sz}	Moment of inertia in z-axis	3.072/kg m ²
k_{dl}	Drag coef. along x,y,z-axis	55×10^{-4} /N s/m
k_{dr}	Drag coef. about x,y,z-axis	55×10^{-4} /N s
k_{p1}, k_{p2}, k_{p3}	Control constants	18, 9, 18
$\beta_1, \beta_2, \beta_3$	Control constants	0.4, 0.4, 0.4
$\zeta_\phi, \zeta_\theta, \zeta_\psi$	Control constants	22, 30, 22
$\varepsilon, \gamma, \kappa_1, \kappa_2$	Control constants	2, 5, 85, 55
\mathcal{M}	Virtual mass	0.95/kg
\mathcal{C}	Virtual damping coef.	1.54/N s/m
\mathcal{K}	Virtual spring constant	0/N s/m

trajectory which will be generated by the admittance controller according to the human operator's guidance through the applied forces $\mathcal{F}_h \in \mathbb{R}^3$. The goal for the aerial system is to hold its position when no external force is applied. Consequently, $\tilde{\mathcal{R}}_d$ and $\tilde{\mathcal{R}}_d$ are set to zero. In addition, the response of the physical interaction can be adjusted by modifying the virtual stiffness \mathcal{K} . A higher value of \mathcal{K} results in a stiffer response, whereas setting \mathcal{K} to zero ensures full-compliance with the applied external force. Furthermore, to mitigate environmental disturbances, the admittance controller is activated when the measured force exceeds a defined threshold.

IV. SIMULATION AND NUMERICAL RESULTS

The control design and the performance of the system which consists of two quadrotors attached to a common payload as shown in Fig. 3.(a) are validated using MATLAB (2024b), Robotic Operation System (ROS) noetic, and Gazebo 11 (see Fig. 3). Table I presents the parameters of the system and the controller. Initially, the aerial vehicle lifted the payload to the operating height, at which the admittance controller was triggered to be ready for physical interaction. The user applied an upward force to properly position the aerial vehicle. Subsequently, simulated human guidance was performed by applying forces in various directions to transport the payload to the final destination. The results indicate that the system was fully complied with the applied human guidance while the controller maintained stability throughout the process until the final destination was reached, as shown in Fig. 3.(b) and 3.(c).

Fig. 4 shows the desired and actual trajectories of the orientation, position, velocity, and tracking errors of the system. The system successfully tracked the reference trajectories that generated by the admittance controller as inputs to the position and attitude controllers. The first column of Fig. 4 shows the desired and actual orientation of the system. It can be clearly seen that the position controller managed to generate the desired orientation to the attitude controller while the latter tracked this desired orientation required to move the system to the positions in the x and (y) directions according to human guidance. In addition, The (z) direction graph illustrates that the system's altitude increased to the desired

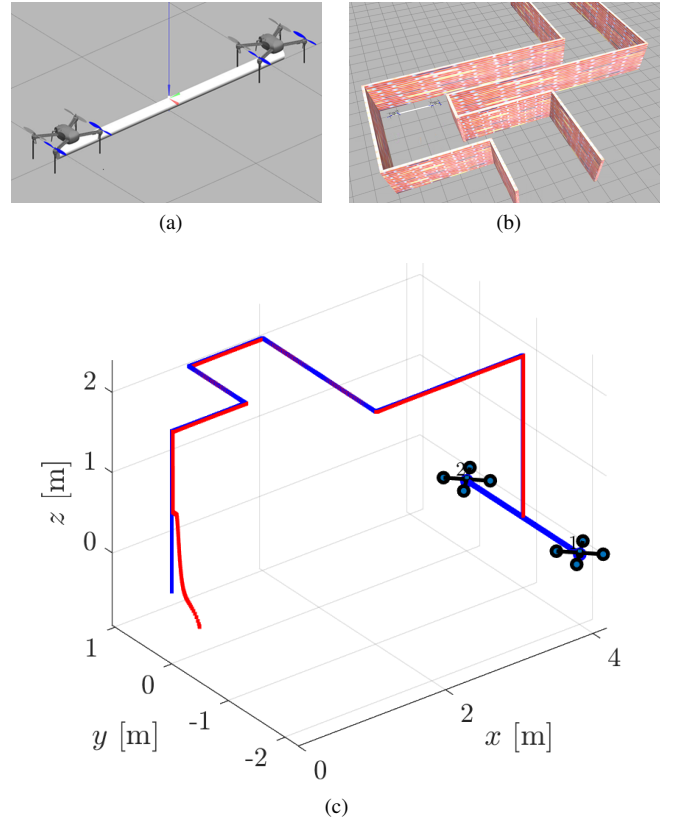


Fig. 3: Simulation; (a) The aerial system built in ROS and Gazebo 11, (b) Zigzag corridor as a navigation workplace, (c) MATLAB simulation with tracking path in 3D space.

altitude, maintained that altitude until the final destination, and then the aerial system was landed. Meanwhile, the velocity graph displays the corresponding required velocities. Fig. 4 further illustrates the normalized tracking errors for the system's position and attitude controllers at the last row of the graph. The results indicate that the position and velocity errors were reduced to zero throughout the simulation, demonstrating the robustness of the proposed controller. In contrast, the orientation error exhibited some fluctuations, likely due to the high rolling and pitching control inputs at the start and stop of the system, which are related to the system's high inertia. However, the controller successfully bounded and reduced the orientation error to zero. Fig. 5 displays the control inputs generated by the controller. The graph of the total thrust \mathcal{U}_{th} shows the required generated thrust to reach the desired altitude and maintaining the same thrust for the desired altitude, then finally generated reverse thrust for landing. The other three graphs show the rolling, pitching, and yawing moments which are required to navigate to the desired positions in 3D space according to human guidance.

V. CONCLUSION

This paper presents control strategy for an aerial cooperative payload transportation system using two quadrotor UAVs rigidly connected to a payload with human physical interaction. The integration of adaptive backstepping control

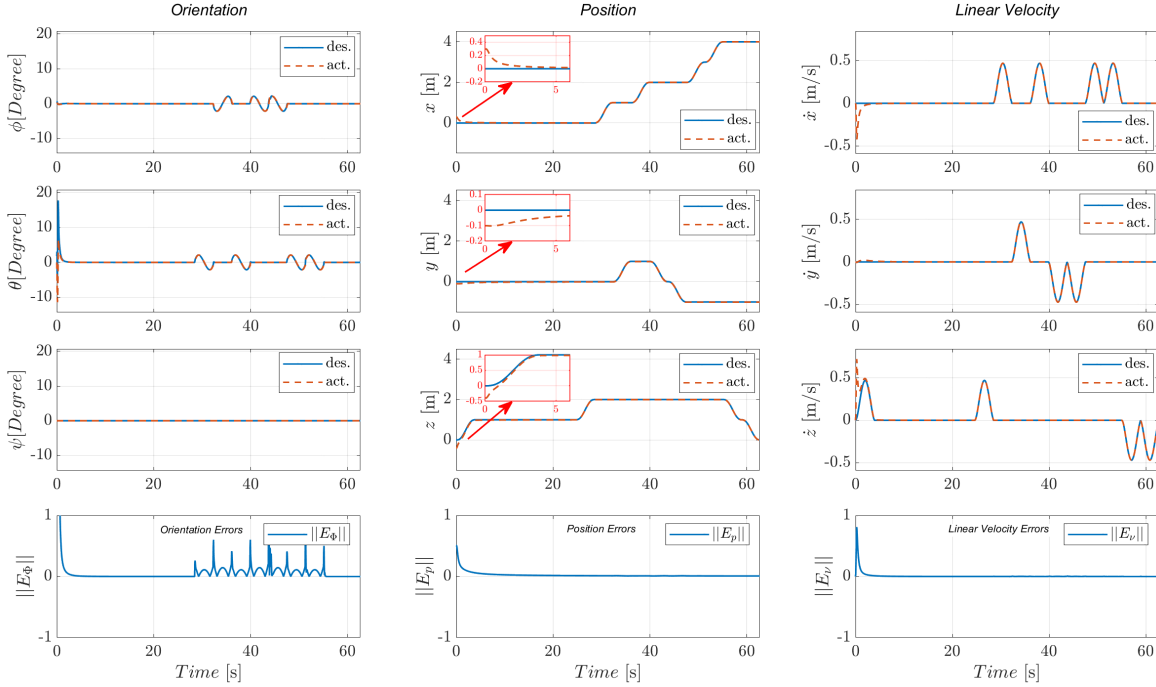


Fig. 4: The simulation results; First column for the desired and actual orientation, Second column for the desired and actual position, Third column for the linear velocity in (x, y, z) directions, and the bottom row for the normalized tracking errors.

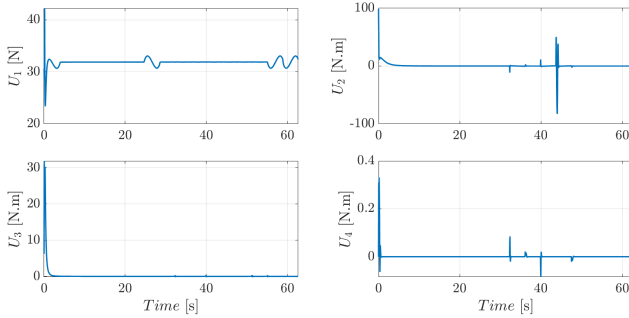


Fig. 5: The control inputs.

for the position subsystem, Fast Nonsingular Terminal Sliding Mode Control (FNTSMC) for the attitude subsystem, and an admittance controller for human interaction ensures precise trajectory tracking. The proposed control design ensures position and attitude asymptotic stabilization with responsive human guidance. Simulation results demonstrate the effectiveness of the proposed method in maintaining system stability and robust performance.

REFERENCES

- [1] H. A. Hashim, "Advances in UAV Avionics Systems Architecture, Classification and Integration: A Comprehensive Review and Future Perspectives," *Results in Engineering*, vol. 25, p. 103786, 2025.
- [2] F. Real and et al., "Experimental evaluation of a team of multiple unmanned aerial vehicles for cooperative construction," *IEEE Access*, vol. 9, pp. 6817–6835, 2021.
- [3] H. A. Hashim, "Exponentially Stable Observer-based Controller for VTOL-UAVs without Velocity Measurements," *International Journal of Control*, vol. 96, no. 8, pp. 1946–1960, 2023.
- [4] D. Hachiya, E. Mas, and S. Koshimura, "A reinforcement learning model of multiple uavs for transporting emergency relief supplies," *Applied Sciences*, vol. 12, no. 20, p. 10427, 2022.
- [5] H. A. Hashim, A. E. Eltoukhy, and K. G. Vamvoudakis, "UWB Ranging and IMU Data Fusion: Overview and Nonlinear Stochastic Filter for Inertial Navigation," *IEEE Transactions on Intelligent Transportation Systems*, vol. 25, no. 1, pp. 359–369, 2024.
- [6] D. K. D. Villa and et al., "Cooperative load transportation with two quadrotors using adaptive control," *IEEE Access*, vol. 9, pp. 129 148–129 160, 2021.
- [7] D. Chaikalis and et al., "Decentralized leader-follower visual cooperative package transportation using unmanned aerial manipulators," in *2023 European Control Conference (ECC)*, 2023, pp. 1–5.
- [8] H. Lee, H. Kim, W. Kim, and H. J. Kim, "An integrated framework for cooperative aerial manipulators in unknown environments," *IEEE Robotics and Automation Letters*, vol. 3, no. 3, pp. 2307–2314, 2018.
- [9] Y. H. Tan, S. Lai, K. Wang, and B. M. Chen, "Cooperative control of multiple unmanned aerial systems for heavy duty carrying," *Annual Reviews in Control*, vol. 46, pp. 44–57, 2018.
- [10] G. Loianno and V. Kumar, "Cooperative transportation using small quadrotors using monocular vision and inertial sensing," *IEEE Robotics and Automation Letters*, vol. 3, no. 2, pp. 680–687, 2018.
- [11] H. Naser, H. A. Hashim, and M. Ahmadi, "Aerial Assistive Payload Transportation using Quadrotor UAVs with Nonsingular Fast Terminal SMC for Human Physical Interaction," *Results in Engineering*, vol. 25, p. 103701, 2025.
- [12] H. A. Hashim and K. G. Vamvoudakis, "Adaptive Neural Network Stochastic-Filter-based Controller for Attitude Tracking with Disturbance Rejection," *IEEE Transactions on Neural Networks and Learning Systems*, vol. 35, no. 1, pp. 1217–1227, 2024.
- [13] M. Romano, A. Ye, J. Pye, and E. Atkins, "Cooperative multilift slung load transportation using haptic admittance control guidance," *Journal of Guidance, Control and Dynamics*, vol. 45, pp. 1899–1912, 2022.
- [14] G. Li, X. Liu, and G. Loianno, "Safety-aware human-robot collaborative transportation and manipulation with multiple mavs," *arXiv preprint arXiv:2210.05894*, 2022.
- [15] G. Li, R. Ge, and G. Loianno, "Cooperative transportation of cable suspended payloads with mavs using monocular vision and inertial sensing," *IEEE Robotics and Automation Letters*, vol. 6, no. 3, pp. 5316–5323, 2021.
- [16] S. Barawkar and M. Kumar, "Cooperative transport of a payload with offset cg using multiple uavs," in *Dynamic systems and control conference*, vol. 59162. American Society of Mechanical Engineers, 2019, p. V003T21A008.

- [17] H. A. Hashim, A. E. Eltoukhy, and A. Odry, "Observer-based Controller for VTOL-UAVs Tracking using Direct Vision-aided Inertial Navigation Measurements," *ISA transactions*, vol. 137, pp. 133–143, 2023.
- [18] H. A. Hashim, "A Geometric Nonlinear Stochastic Filter for Simultaneous Localization and Mapping," *Aerospace Science and Technology*, vol. 111, p. 106569, 2021.
- [19] J.-J. Xiong and G.-B. Zhang, "Global fast dynamic terminal sliding mode control for a quadrotor uav," *ISA transactions*, vol. 66, pp. 233–240, 2017.
- [20] M. Labbadi and et al., "Barrier Function-based Adaptive Nonsingular Fast Terminal Sliding Mode Control for Disturbed UAVs," in *2022 European Control Conference (ECC)*. IEEE, 2022, pp. 975–980.
- [21] H. A. Hashim, "Special Orthogonal Group SO(3), Euler Angles, Angle-axis, Rodriguez Vector and Unit-quaternion: Overview, Mapping and Challenges," *arXiv preprint arXiv:1909.06669*, 2019.
- [22] R. Babaie and A. F. Ehyai, "Robust optimal motion planning approach to cooperative grasping and transporting using multiple uavs based on sdre," *Transactions of the Institute of Measurement and Control*, vol. 39, no. 9, pp. 1391–1408, 2017.
- [23] M. Boukattaya, N. Mezghani, and T. Damak, "Adaptive nonsingular fast terminal sliding-mode control for the tracking problem of uncertain dynamical systems," *ISA transactions*, vol. 77, pp. 1–19, 2018.